ACS APPLIED MATERIALS & INTERFACES

Research Article

Cite This: ACS Appl. Mater. Interfaces XXXX, XXX, XXX−XXX

www.acsami.org

Overcoming Chemoresistance in Cancer via Combined MicroRNA Therapeutics with Anticancer Drugs Using Multifunctional Magnetic Core−Shell Nanoparticles

Perry T. Yin,[†,¶] Thanapat Pongkulapa,[‡,¶] Hyeon-Yeol Cho,[‡,§] Jiyou Han,[∥,⊥] Nicholas J. Pasquale,[‡] Hudifah Rabie,[‡] Jong-Hoon Kim,[∥] Jeong-Woo Choi,[§] and Ki-Bum Lee*[,†,‡,#]

[†]Department of Biomedical Engineering and [‡]Department of Chemistry and Chemical Biology, Rutgers, The State University of New Jersey, Piscataway, New Jersey 08854, United States

[§]Department of Chemical and Biomolecular Engineering, Sogang University, Seoul 04107, Republic of Korea

[∥]Division of Biotechnology, Laboratory of Stem Cells and Tissue Regeneration, College of Life Sciences and Biotechnology, Korea University, Seoul 02841, Republic of Korea

[⊥]Department of Biological Sciences, Laboratory of Stem Cell Research and Biotechnology, Hyupsung University, Hwaseong-si 18330, Republic of Korea

[#]College of Pharmacy, Kyung Hee University, 26 Kyungheedae-ro, Dongdaemun-gu, Seoul 02447, Korea

Supporting Information

ABSTRACT: In this study, we report the use of a multifunctional magnetic core−shell nanoparticle (MCNP), composed of a highly magnetic zinc-doped iron oxide ($ZnFe_2O_4$) core nanoparticle and a biocompatible mesoporous silica (mSi) shell, for the simultaneous delivery of let-7a microRNA (miRNA) and anticancer drugs (e.g., doxorubicin) to overcome chemoresistance in breast cancer. Owing to the ability of let-7a to repress DNA repair mechanisms (e.g., BRCA1 and BRCA2) and downregulate drug efflux pumps (e.g., ABCG2), delivery of let-7a could sensitize chemoresistant breast cancer cells (MDA-MB-231) to subsequent doxorubicin chemotherapy both in vitro and in vivo. Moreover, the multifunctionality of our MCNPs allows for the monitoring of in vivo delivery via magnetic resonance imaging. In short, we have developed a multifunctional MCNP-based therapeutic approach to provide an attractive method with which to enhance our ability not only to deliver combined miRNA therapeutics with small-molecule drugs in both selective and effective manner but also to sensitize cancer cells for the enhanced treatment via the combination of miRNA replacement therapy using a single nanoplatform.

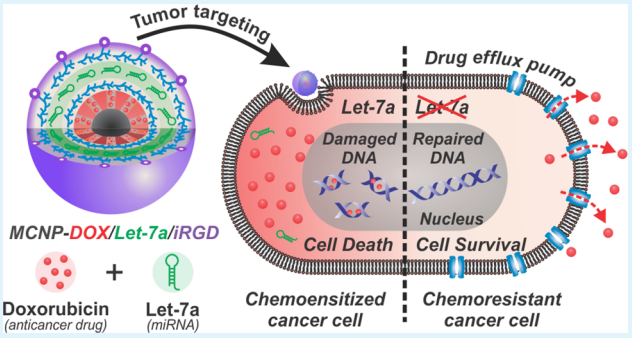

KEYWORDS: *magnetic core−shell nanoparticles, microRNA therapeutics, chemoresistance, targeted delivery, combination cancer therapy*

INTRODUCTION

Cancer is a complex disease that is characterized by the existence of a multitude of genetic and epigenetic alterations that promote cellular abnormalities such as aggressive growth and resistance to apoptosis.[1] Breast cancer, which is the most frequently diagnosed cancer in women in the United States, is typically divided into histological subtypes based on the expression of specific receptors such as the estrogen receptor, progesterone receptor, and human epidermal growth factor receptor (HER2) or the absence of all three (e.g., triple-negative breast cancer).[2,3]

The conventional treatment for breast cancer depends on the subtype but typically involves surgical resection of the tumor followed by adjuvant radiotherapy and chemotherapy. For example, the most frequently used chemotherapeutic regimens for breast cancers are based on anthracyclines [doxorubicin (DOX), daunomycin, and epirubicin][4] and taxanes [paclitaxel and docetaxel].[5,6] However, current chemotherapeutic strategies to treat breast cancers often cannot account for the vast degree of heterogeneity that exists within the tumor. Moreover, breast cancer cells often acquire chemoresistance, failing to eradicate the entire tumor and recurrence, especially in patients with triple-negative breast cancer. One common way by which cancer acquires drug resistance is the overexpression of drug transporters [e.g., adenosine triphosphate-binding cassette (ABC) transporters]. Other mechanisms through which cancer develops chemoresistance include aberrations of DNA damage response

Received: June 1, 2018
Accepted: July 20, 2018
Published: July 20, 2018

DOI: 10.1021/acsami.8b09086
ACS Appl. Mater. Interfaces XXXX, XXX, XXX−XXX

Scheme 1. Design and Functions of the Multifunctional MCNP Construct for Combined miRNA Therapeutics and Anticancer Drugs To Overcome Chemoresistance[a]

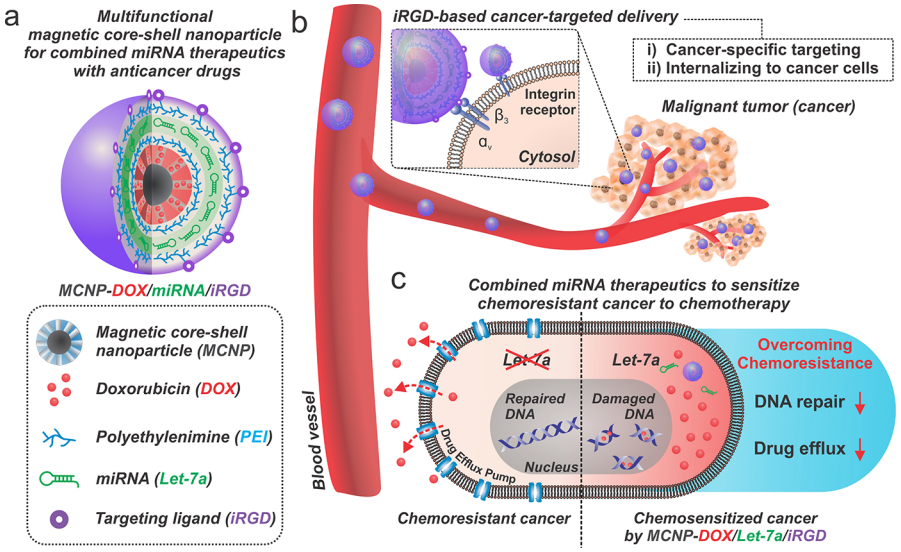

[a](a) Design of the MCNP construct for simultaneous delivery of miRNA and anticancer drugs (e.g., DOX). (b) MCNP construct is decorated with iRGD peptide, enabling the tumor-targeted delivery via $\alpha_V\beta_3$ integrin-mediated uptake. (c) Codelivery of miRNA (let-7a) sensitizes cancer cells to DOX therapy via inhibition of multiple chemoresistance-related genes, including those associated in drug efflux and DNA repair mechanisms.

pathways as well as activation of alternative signaling pathways, resulting in cancer cell survival and evasion from cell death. Hence, there is a critical need for novel approaches that can simultaneously regulate a broad set of chemoresistance-related genes, especially those responsible for prosurvival pathways, DNA repair mechanisms, and drug efflux pumps, thereby sensitizing cancer cells to subsequent treatment with conventional chemotherapies and enhancing cancer apoptosis.[7]

To this end, combining microRNA (miRNA) therapeutics with anticancer drugs using multifunctional magnetic core–shell nanoparticles (MCNPs) would be a powerful approach. miRNAs are short (20–22 nucleotides) noncoding RNA molecules that bind to messenger RNAs (mRNAs) in a completely or partially complementary fashion, leading to the degradation or translational inhibition of the mRNA targets.[8−10] miRNAs have already been known to play a significant role in developmental biology as well as in stem cell biology.[11,12] A growing body of evidence suggests that mutations in miRNA can cause the development and/or progression of cancer.[9,13] For example, **let-7a** miRNA (let-7a), which is reduced in brain, breast, lung, and ovarian cancers, is hypothesized to be a tumor suppressor that inhibits cancer growth by reducing oncogene expression (e.g., RAS and HMGA2).[14] Therefore, miRNA replacement therapy is emerging as a promising treatment approach for cancers such as those of the breast. Although miRNA-based therapies have great clinical potential, possible synergies with conventional chemotherapeutic agents remain poorly explored. Furthermore, their wide applications are significantly hampered by the lack of appropriate delivery platforms and corresponding molecular imaging methods.

In this paper, we demonstrate the use of a multifunctional MCNP, composed of a highly magnetic zinc-doped iron oxide ($ZnFe_2O_4$) core and a biocompatible mesoporous silica (mSi) shell, as a vehicle for the simultaneous delivery of let-7a with the anticancer drug (DOX) to breast cancer cells, thereby effectively overcoming chemoresistance (Scheme 1). The multifunctionality of our MCNPs allows for the conjugation of tumor-targeting/penetrating peptides, such as iRGD (internalizing RGD, C**RGD**KGPDC), as well as the ability to monitor drug delivery via fluorescence and magnetic resonance imaging (MRI). Moreover, although let-7a has primarily been shown to inhibit the malignant growth of cancer cells by targeting RAS and HMGA2, it is also known to have functions in DNA repair (e.g., BRCA1 and BRCA2), cell cycle, and regulate multidrug resistance genes/drug efflux pumps (e.g., ABCG2).[15] As such, using a triple-negative breast cancer cell line (e.g., MDA-MB-231) as a model system, we hypothesized that the codelivery of let-7a as a replacement therapy could sensitize these breast cancer cells to subsequent DNA-damaging agents such as DOX. Collectively, our developed MCNP-based therapeutic approach can provide an attractive means with which to enhance our ability to not only deliver and monitor multiple therapeutics but also sensitize cancer cells for enhanced treatment via combinatorial miRNA replacement therapy using a single nanoplatform.

EXPERIMENTAL SECTION

Synthesis and Characterization of the Core–Shell Nanoparticle. The $ZnFe_2O_4$ magnetic core with mSi shell nanostructure was prepared and characterized according to the protocol previously reported by our and other's groups.[16−23]

DOX Loading and Release Kinetics from MCNP. Prior to DOX loading, the MCNPs were postgrafted with trihydroxysilylpropyl methylphosphonate (THMP) to create phosphonate ($-PO_3^-$)-modified MCNPs, using a postgrafting method that was adopted from a previous report.[24] After functionalization with $-PO_3^-$, the MCNPs were dispersed in an aqueous solution of DOX such that the final concentration of DOX and nanoparticle was 1 mg/mL. The solution was then stirred overnight for DOX loading. Next, branched polyethylenimine (PEI) (M_n = 10 000 kDa) was added such that the final PEI concentration was 10 mg/mL, along with NaCl solution at the final concentration of 1 mM. This molecular weight and structure of PEI were chosen based on previous reports.[25] The solution was stirred for at least half an hour and then purified by centrifugation at 10 000 rpm for 10 min. Purification was performed twice; then, the

DOI: 10.1021/acsami.8b09086
ACS Appl. Mater. Interfaces XXXX, XXX, XXX−XXX

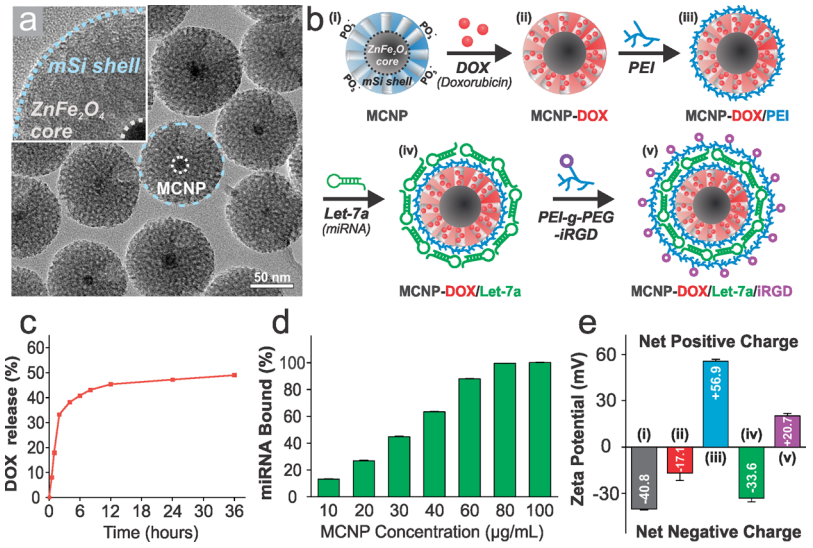

Figure 1. Synthesis and characterization of the multifunctional MCNPs for codelivery of miRNA and anticancer drugs. (a) HR-TEM image of MCNPs (scale bar = 50 nm) composed of a highly magnetic zinc-doped iron oxide nanoparticle ($ZnFe_2O_4$) core and a biocompatible mSi shell. (b) Schematic illustration depicting layer-by-layer assembly of the multifunctional MCNP construct for codelivery of miRNA and DOX: (i) phosphonate (PO_3^-)-functionalized MCNP; (ii) DOX-loaded MCNPs (MCNP-DOXs); (iii) PEI-coated MCNP-DOX construct (MCNP-DOX/PEI); (iv) Let-7a-complexed MCNP-DOX/PEI (MCNP-DOX/Let-7a); and (v) PEI-*g*-PEG-iRGD-coated MCNP-DOX/Let-7a construct (MCNP-DOX/Let-7a/iRGD). (c) In vitro DOX release kinetics of DOX-loaded MCNPs (MCNP-DOXs) in PBS (pH 7.4). (d) miRNA loading efficiency of MCNPs at different concentrations determined by quantification assay using PicoGreen dye (miRNA concentration = 100 nM). (e) Stepwise layer-by-layer process of the MCNP constructs was confirmed by tracking changes in the zeta potential. All of the measurements were performed in triplicate (n = 3).

DOX-loaded MCNPs (MCNP-DOXs) were dispersed in Dulbecco's phosphate-buffered saline (DPBS) and used immediately. The loading and encapsulation efficiency are calculated based on the equations previously reported.[26]

To study the release kinetics, MCNP-DOXs (20 mg) were incubated in 20 mL of DPBS (pH 7.4) under stirring. At different time points, a portion of the solution (1 mL) was collected for centrifugation. The absorption of the supernatant was measured by a UV−visible spectrometer (Varian Cary 50 spectrophotometer, CA) using maximum absorption of DOX at 480 nm. The DOX content in the solution was determined by a standard curve.[27]

Formation of MCNP-DOX/miRNA Constructs. The following miRNAs were purchased from Ambion (MA): let-7a (AM17100), control miRNA (AM17110), and Cy3 dye-labeled control miRNA (AM17120).

To prepare the MCNPs for miRNA delivery, the DOX-loaded MCNPs (MCNP-DOXs) were coated with a cationic polymer, branched PEI, to afford PEI-coated MCNP-DOXs with an overall positive charge. To complex miRNA, PEI-coated MCNP-DOXs were mixed with 100 nM miRNA in 80 mM NaCl aqueous solution. The presence of NaCl in the solution was necessary to overcome repulsive forces and to facilitate the binding of miRNA and PEI polymer around the MCNPs.[28] After incubation for 20 min at room temperature, the samples were filtered using a centrifugal filter unit (MilliporeSigma, NY, MWCO = 10 000 Da) to remove excess PEI and yield MCNP/miRNA or MCNP-DOX/miRNA constructs. To determine the miRNA loading capacity of MCNPs, different concentrations (10−100 μg/mL) of PEI-coated MCNPs were first incubated in 100 nM miRNA solution. Afterward, a PicoGreen dye solution (1:200 dilution in Tris−EDTA buffer) was added and fluorescence measurements were made. All measurements were corrected for background fluorescence using a solution containing only buffer and PicoGreen dye. The hydrodynamic size and zeta potential of the MCNP constructs were assessed by dynamic light scattering (DLS) measurements [Malvern Instruments Zetasizer Nano ZS-90 (Southborough, MA)]. Detailed measurement conditions can be found in our previous report.[22]

Preparing MCNP Constructs for Tumor Targeting. The PEI-*g*-PEG-iRGD conjugates were synthesized via a two-step reaction as described previously (Scheme S1).[29,30] Then, the as-prepared MCNP-DOX/miRNA constructs were coated with the PEI-*g*-PEG-iRGD conjugates to obtain the tumor-targeting MCNP-DOX/miRNA/iRGD construct.

Transfection of Cell Lines with MCNP Constructs. Breast cancer cells (MDA-MB-231 and MCF-7 obtained from ATCC, VA) were seeded into each well of a 12-well plate to attain 80% confluency (30 000 cells in a volume of 500 μL) in growth medium [Dulbecco's modified Eagle's medium (DMEM) supplemented with 10% fetal bovine serum (FBS) and 1% penicillin−streptomycin]. After incubation for 24 h, the desired amount of the MCNP construct was mixed with reduced serum media, Opti-MEM (Life Technologies, MA), and added to each well. Subsequently, the cell culture plates were subject to magnetofection on a Nd−Fe−B magnet (OZ Biosciences, France) for 10 min, as optimized from previous report.[19] The culture plates were then removed from the magnet and incubated for 5 h. Afterward, the transfected cells were washed with DPBS, followed by replacing with fresh growth medium.

Cell Viability Assays. The percentage of viable cells was determined 48 h after transfection by 3-(4,5-dimethylthiazol-2-yl)-5-(3-carboxymethoxyphenyl)-2-(4-sulfophenyl)-2*H*-tetrazolium assay. The emitted fluorescence signal was collected at 590 nm with 560 nm excitation. All measurements were repeated in triplicate and normalized to the nontreated condition.

Gene Expression Analysis. The total RNA was isolated 48 h after initial transfection using TRIzol Reagent (Life Technologies, MA). The conversion of total RNA to cDNA was accomplished using SuperScript III First-Strand Synthesis System (Life Technologies, MA). The mRNA expression level of genes of interest was analyzed using quantitative PCR (qPCR) and reported in fold change values relative to control as described previously.[22,23] The standard cycling conditions were used for all reactions with a melting temperature of 60 °C. Primers are listed in Table S1. All primers were obtained from the PrimerBank.[31−33]

Animal Studies. Six week-old BALB/c nude mice were purchased from RaonBio (Yongin-si, Gyeonggi-do, Republic of Korea). All

DOI: 10.1021/acsami.8b09086
ACS Appl. Mater. Interfaces XXXX, XXX, XXX−XXX

animals were acclimated at least 48 h prior to experiment and maintained according to the guidelines published by the National Institute of Health (NIH). The animal facility was kept under 12 h light/dark cycles at room temperature 21 ± 2 °C with 30−40% humidity. MDA-MB-231 cells (5.0×10^6) were mixed with matrigel (BD Biosciences, CA) and were transplanted in both flanks or shoulders via subcutaneous (SC) injection.[34,35] Treatments of nanoparticles were injected either via intravenous (IV) injection or through intratumoral (IT) injection, and the injection volume was 50 μL/site. In vivo imaging system (IVIS) spectrum (PerkinElmer, Waltham, MA) was used to monitor the fluorescence emitted from the fluorescein isothiocyanate (FITC)-labeled MCNPs. For ex vivo images, the tumor tissues and other organs (lung, heart, liver, kidney, and spleen) of all of the animals were extracted after cervical dislocation under anesthesia and measured using IVIS. The fluorescence images were processed with commercial software (Living Image software for IVIS spectrum/200, ver. 4.1, Waltham, MA).

MRI Experiment. The magnetic resonance images were acquired under anesthesia on a 4.7 T MRI scanner with the following parameters: field of view = 5 × 3 cm^2, matrix size = 256 × 256, slice thickness = 1 mm, echo time (TE) = 10 ms, and repetition time (TR) = 350 ms.

RESULTS AND DISCUSSION

Design and Synthesis of the MCNP-Based Codelivery of miRNA and Anticancer Drug. To deliver let-7a and DOX simultaneously, we first synthesized multifunctional MCNPs with a $ZnFe_2O_4$ magnetic nanoparticle core and a biocompatible mSi shell. A $ZnFe_2O_4$ core was chosen as it has previously been reported to have a significantly higher saturation magnetization as well as relaxation for improving MRI contrast when compared to conventional Fe_2O_3 or Fe_3O_4 magnetic nanoparticles.[16,36] To this end, we first synthesized the magnetic cores via thermal decomposition of a mixture of metal precursors.[16,19] High-resolution transmission electron microscopy (HR-TEM) revealed the average diameter of the as-synthesized MCNPs, which was 93.88 ± 7.40 nm with a 11.88 ± 2.03 nm core and a 38.45 ± 3.44 nm thick mSi shell (Figure 1a). Moreover, the $ZnFe_2O_4$ cores exhibited a monocrystalline structure with a lattice fringe of 4.8 Å (Figure S1a), which corresponds to the (111) plane of the $ZnFe_2O_4$ spinel.[16,19] Following further modification of the MCNPs, it was confirmed that the cetrimonium bromide (CTAB) template had been extracted from the 3 nm-sized pore of the mSi shell via Fourier transform infrared spectroscopy (FTIR) analysis (Figure S1b).

To efficiently deliver anticancer drugs, DOX was loaded in the pores of the mSi shell of the MCNPs (Figure 1b). To this end, the pores were first functionalized with phosphonate ($-PO_3^-$) groups using the postgrafting method from a previously described protocol that was modified by our group.[26,37] In particular, this been shown to enhance the loading of DOX via electrostatic interactions.[26] Briefly, the as-synthesized MCNPs were subjected to postgrafting of THMP. To characterize surface functionalization with THMP, the zeta potential of the MCNPs was measured in different pH environments (Figure S1c).

The increase in the negative surface potential of the phosphonate-modified MCNP compared to the nonmodified MCNPs confirmed successful modification.[26] To upload DOX onto MCMPs, the phosphonate-modified MCNPs were added to the DOX solution (1 mg/mL) and incubated overnight under stirring. The mixture was then centrifuged to isolate the DOX-loaded MCNPs (MCNP-DOXs). The DOX loading efficiency of the phosphonate-modified MCNP was found to be 12.1% with an encapsulation efficiency of 48.7%, which is significantly higher than nonmodified MCNPs (loading efficiency = 2.1%, encapsulation efficiency = 8.4%).[38] Moreover, the release profile of the MCNP-DOXs was determined in PBS at pH 7.4, showing a cumulative release of 49% (Figure 1c), which agrees with previous reports.[26]

Prior to utilizing the as-synthesized MCNPs for miRNA delivery, a PEI layer was introduced to the MCNP surface via electrostatic interactions between the opposite charges. As a result, the positively charged surface of the PEI-coated MCNPs will permit complexation of the MCNPs with miRNA via layer-by-layer assembly. It was found that the hydrodynamic size of the PEI-coated MCNPs increased slightly to 99.75 ± 36.83 nm [polydispersity index (PDI) = 0.177] as measured by DLS. On the other hand, a significant change in zeta potential was observed (+56.90 ± 1.27 mV), which confirmed the successful adsorption of PEI on the MCNP surface (Figure S1d). It is known that the toxicity of PEI as a gene delivery material is directly linked to its structure and molecular weight.[39,40] Therefore, to mitigate this cytotoxicity while maintaining a high transfection efficiency, we selected 10 kDa branched PEI, which has been reported to have good biocompatiblilty.[22,41] It was found that our PEI-coated MCNPs were nontoxic to breast cancer cells up to 200 μg/mL, with 100 μg/mL resulting in over 95% cell viability (Figure S1e).

To load miRNAs onto our MCNPs, we utilized a layer-by-layer process (Figure 1b). The positively-charged MCNPs (PEI-coated) were complexed with the negatively-charged miRNA molecules via electrostatic interaction to yield miRNA-complexed MCNP constructs (MCNP/miRNA). To assess the miRNA loading capacity of the MCNPs, a fixed concentration of miRNA (100 nM) was mixed with different concentrations of MCNPs to form MCNP/miRNA constructs. Subsequently, the unbound miRNA left in the supernatant was determined using PicoGreen dye to identify the concentration of MCNPs on which the entire miRNA can fully be adsorbed. We found that 100 nM of miRNA could fully complex with 100 μg/mL MCNP (Figure 1d), which is in the nontoxic range of our MCNPs. Next, we observed that the size of the MCNP/miRNA constructs increased to a final diameter of 107 ± 22.35 nm (PDI = 0.433) and had a net negative zeta potential of −33.6 ± 8.62 mV (Figure S1d). Lastly, the MCNP/miRNA constructs were coated with an outer layer of PEI to provide a net positive surface charge to not only facilitate cellular uptake and endosomal escape based on the proton sponge effect[42,43] but also allow modification with tumor-targeting/penetrating moieties, that is iRGD peptide, via facile bioconjugation of the amine groups on the surface of the PEI. The progression of layer-by-layer assembly on the MCNPs was characterized by tracking the surface charge potential after each step of layer-by-layer assembly and is summarized in Figure 1e. The layer-by-layer construct exhibited good stability in deionized water and cell culture media (10% FBS in DMEM) over the period of 5 days, which was sufficient for localization at the tumor location after the injection into the body (Figure S2).

Improving Cellular Uptake and Anticancer Efficacy Using MCNP-DOX/miRNA Codelivery. To assess the efficiency of nanoparticle cellular uptake and the ability to simultaneously deliver miRNA and anticancer drug, we performed fluorescence imaging analysis on MDA-MB-231 cells that were transfected with DOX-loaded and miRNA-complexed MCNP constructs (MCNP-DOX/miRNA). Specifically, DOX and Cy3 dye-labeled miRNA were loaded onto the

DOI: 10.1021/acsami.8b09086
ACS Appl. Mater. Interfaces XXXX, XXX, XXX−XXX

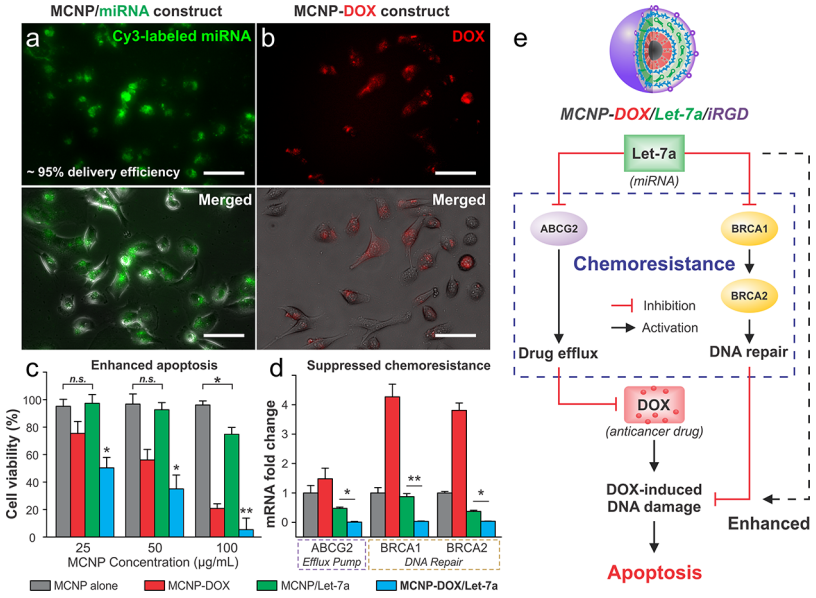

Figure 2. Synergistic anticancer effect of codelivery of miRNA and DOX via multifunctional MCNPs. (a,b) Cellular uptake of (a) Cy3-labeled miRNA-complexed and (b) DOX-loaded MCNPs was confirmed in MDA-MB-231 cells by fluorescence imaging (scale bar = 50 μm). (c) Concentration-dependent cytotoxicities of MCNPs (gray), DOX-loaded MCNPs [MCNP-DOX] (red), let-7a-complexed MCNPs [MCNP/Let-7a] (green), and let-7a-complexed with DOX-loaded MCNPs [MCNP-DOX/Let-7a] (blue) were assessed 48 h after treatment. (d) Quantitative reverse transcription PCR (RT-qPCR) showed significant downregulation of target genes involved in chemoresistance-related genes, including drug efflux pumps (ABCG2) and DNA repair (BRCA1/BRCA2), after 48 h treatment with MCNP-DOX/Let-7a compared to either modality alone. (n = 3; n.s. = not significant, *p < 0.05, **p < 0.001). (e) Schematic diagram of proposed chemoresistant mechanisms that are synergistically inhibited by let-7a to enhance DOX-induced apoptosis.

MCNPs, and the delivery process was enhanced by magnetofection to facilitate rapid accumulation of MCNP-DOX/miRNA constructs onto the cell membrane. After 24 h, we found that the constructs were efficiently uptaken by the cells as evidenced by the presence of intracellular fluorescent signals from the Cy3 dye-labeled miRNA (green) and DOX (red) (Figure 2a,b).

To systematically evaluate the anticancer efficacy of our combined therapeutics, we first delivered MCNP-DOXs (i.e., DOX alone without miRNA) into MDA-MB-231 cells. The treatment of MDA-MB-231 cells with MCNP-DOXs resulted in a clear decrease of cell viability in a dose-dependent manner, wherein 100 μg/mL MCNP-DOXs induced cell apoptosis (~80%) (Figure 2c). Although DOX treatment activates caspase-3-mediated apoptosis, it can also lead to the upregulation of ABCG2 (drug efflux pump) and BRCA1/BRCA2 (DNA repair mechanism) expression, which was confirmed by our qPCR measurements (Figures 2d and S3) and the literature.[44,45] This suggests that there is significant room to improve the anticancer efficacy of DOX treatment on breast cancer cells by simultaneously inhibiting these pathways using miRNA replacement therapy.

Let-7a has been widely explored for its role as a tumor suppressor, targeting many gene transcripts involved in cell survival (PI3K via IGF1R),[46,47] proliferation (RAS, HMGA2),[48,49] and DNA repair (BRCA1, BRCA2).[22,50] For breast cancer, previous studies have shown that let-7 primarily acts to inhibit proliferation and self-renewal through the downregulation of HRAS and HMGA2.[51,52] As such, we delivered MCNP/Let-7a constructs (i.e., let-7a alone without DOX) to MDA-MB-231 cells to evaluate its therapeutic potential. We found that let-7a alone did not cause any significant cytotoxic effect to the cells after 48 h of treatment (Figure S4a). However, using qPCR, we confirmed that let-7a did act primarily through the downregulation of HRAS and HMGA2, whereby these genes were downregulated by over 60% (Figure S4b). Furthermore, the gene targets (ABCG2, BRCA1, and BRCA2) associated with chemoresistance were downregulated to a comparable extent in MDA-MB-231 cells (Figures 2d and S4b). As such, this suggested that our MCNPs were able to deliver miRNA intracellularly and that codelivery of let-7a with DNA-damaging agents such as DOX could potentially induce a synergistic effect via suppression of chemoresistance-related genes.[44]

To test our hypothesis, we exploited the ability of our MCNPs to simultaneously deliver DOX and let-7a to MDA-MB-231 cells using the MCNP-DOX/Let-7a constructs. The cell viability was then assayed 48 h after initial transfection. As expected, we observed a dose-dependent decrease in MDA-MB-231 cell viability with 100 μg/mL MCNP-DOX/Let-7a by over 90% (Figure 2c), which is significantly greater than either treatment modality alone (p < 0.001). To investigate the underlying mechanism of this synergy, qPCR was performed for MDA-MB-231 cells that had been exposed to the combination therapy. It was determined that the combination of DOX and let-7a results in significant downregulation of chemoresistance genes, specifically, drug efflux pump (e.g., ABCG2) and DNA repair mechanisms (e.g., BRCA1 and BRCA2), as well as the other let-7a targets (Figures 2d and S5). This suggests that the MDA-MB-231 cells were sensitized to DOX via an increase in intracellular DOX accumulation as well as DOX-induced DNA damage, which led to higher levels of apoptosis induction (Figure 2e).

Breast Tumor-Targeted Drug Delivery of iRGD-Based MCNP Constructs. Prior to determining the in vivo therapeutic efficacy of our tumor-targeted MCNP-based combination therapy, we decorated the outer PEI layer of our MCNP constructs with a combination of polyethylene

DOI: 10.1021/acsami.8b09086
ACS Appl. Mater. Interfaces XXXX, XXX, XXX−XXX

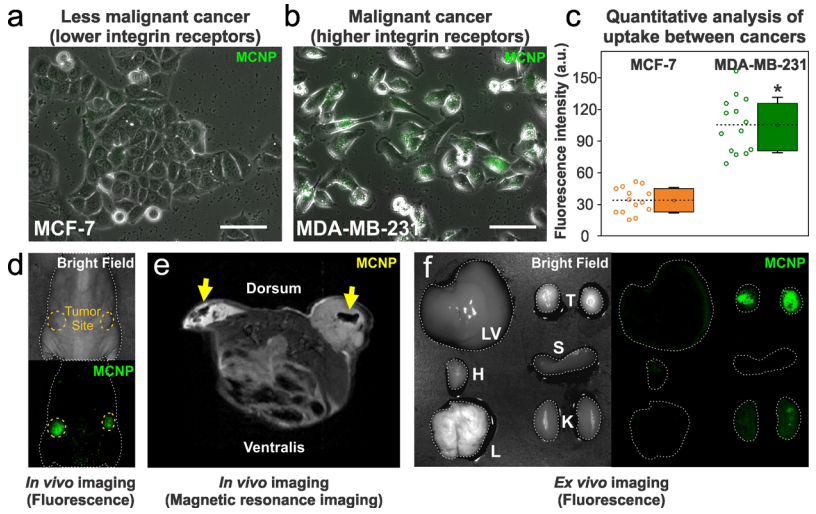

Figure 3. iRGD-mediated tumor targeting of multifunctional MCNP-based miRNA codelivery. (a,b) Cancer-specific internalization of iRGD-conjugated MCNPs (MCNP/iRGD) was determined by delivery of FITC-labeled MCNP/iRGD constructs to (a) MCF-7 cells, which are known to express lower integrin levels than (b) MDA-MB-231 cells. The higher intracellular fluorescent signal was detected from MDA-MB-231 cells because of the higher uptake of FITC-labeled MCNP constructs by the cells. (c) Statistical analysis of fluorescent signals obtained from MCF-7 and MDA-MB-231 cells treated with the constructs (*$p < 0.001$). (d,e) In vivo imaging confirmed the tumor-targeting capability of the MCNP/iRGD constructs 24 h post intravenous injection by (d) fluorescence imaging and (e) MRI. The yellow arrows indicated the accumulation of MCNPs within the tumors. (f) Ex vivo fluorescence imaging also confirmed the targeting capability of MCNP/iRGD constructs toward tumor tissues (LV = liver, T = tumor, H = heart, S = spleen, L = lung, and K = kidney).

glycol (PEG) and iRGD, namely, PEI-*g*-PEG-iRGD (Scheme S1), to form MCNP/iRGD constructs.[53] In particular, PEG was selected as its function as a stealth polymer that suppresses nonspecific interactions with the body [e.g., decreased interactions with blood components (opsonization) that activate the complement system][54] and is endowed with either a slightly negative or slightly positive charge to minimize overall self−self and self−nonself interactions. To impart tumor-targeting modalities, we used iRGD, which is a peptide that has unique cell targeting and tissue-penetrating properties that binds to α_V-integrins. These integrins are commonly overexpressed in the tumor endothelium, including in breast cancers.[55] Moreover, overexpression of $\alpha_V\beta 3$ receptor is found to be higher in malignant cancer cells that are prone to aggressive proliferation and metastasis compared to non-malignant cancer.[56]

To test our MCNP/iRGD, we labeled the construct with FITC via amine-isothiocyanate covalent conjugation. Following this, the FITC-labeled MCNP/iRGD constructs were delivered to two breast cancer cell lines in vitro: MCF-7 cells, which have previously been shown to have low integrin levels, and MDA-MB-231 cells, which are much more aggressive/invasive and highly express integrins.[57] By visualizing FITC using fluorescence microscopy, it was observed that the FITC-labeled MCNP/iRGD constructs were efficiently delivered into MDA-MB-231 cells (90% delivery efficiency), whereas a lower amount was delivered into the MCF-7 cells (30% delivery efficiency) (Figure 3a,b), which was also confirmed by the literature.[57] The fluorescence quantification showed that significantly higher signals were obtained from MDA-MB-231 cells (105.3 ± 6.7 a.u.) when compared to those from MCF-7 cells (33.9 ± 3.1 a.u.) (Figure 3c).

Next, we examined the tumor-targeted delivery of the MCNP/iRGD constructs in vivo. For this purpose, two tumors were generated in each BALB/c nude mouse via subcutaneous injections of MDA-MB-231 cells into both flanks. FITC-labeled MCNP/iRGD constructs were used, whereas FITC-labeled MCNPs were designated as the control. In this case, the FITC-labeled, MCNP/iRGD and control MCNPs were injected via intravenous injection (100 μL of 1 mg/kg). Images were taken 24 h post injection using an IVIS to monitor fluorescence as well as MRI owing to the MRI contrast ability of the $ZnFe_2O_4$ magnetic core. Evidently, only the MCNP/iRGD constructs localized at the sites of the tumors as confirmed using fluorescence imaging and MRI (Figure 3d,e). To confirm biodistribution, the tumors and other organs were extracted after the animals were euthanized for ex vivo fluorescence imaging (Figure 3f). It was determined that the FITC-labeled MCNP/iRGD constructs primarily accumulate in the tumors. Furthermore, we can utilize the magnetic properties to improve the target specificity in the particle delivery by using the magnetic targeting method.[43,58]

In Vivo Anticancer Efficacy of MCNP-Based Combined miRNA and DOX Therapy. On the basis of these results, we sought to determine the therapeutic efficacy of our MCNP platform. The MDA-MB-231 xenografted nude mice were treated with MCNP-DOX/Let-7a/iRGD constructs (combined DOX and let-7a condition) every 3 days for 5 weeks. To directly compare the four different conditions in a single system, a mouse model was generated, wherein each mouse bears four tumor xenografts at both flanks and shoulders (Figure 4a). The particle dose to each animal was 5 mg/kg (DOX, 0.6 mg/kg; miRNA, 129.3 μg/kg) for each injection. The PBS (nontreated condition) and single modality conditions (MCNP-DOXs, DOX alone condition; MCNP/Let-7a, let-7a alone condition) were used as controls. Following euthanasia of the mice after 5 weeks, treatment with MCNP-DOX/Let-7a/iRGD constructs showed a significantly higher rate of tumor inhibition (85% decrease in tumor volume), compared to DOX alone (17% decrease in tumor volume) or let-7a alone (61% decrease in tumor volume) (Figure 4b). We did not observe any decrease in body weight

DOI: 10.1021/acsami.8b09086
ACS Appl. Mater. Interfaces XXXX, XXX, XXX−XXX

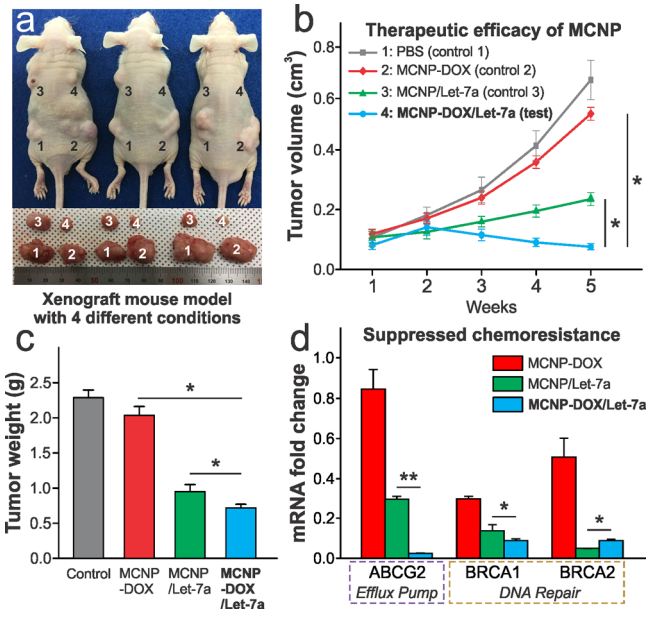

Figure 4. In vivo anticancer efficacy of multifunctional MCNP-based combined miRNA and DOX therapy. (a) Images of tumor-bearing nude mice and dissected tumors from xenografts treated with four different conditions: (1) PBS (control); (2) DOX-loaded MCNP (MCNP-DOX); (3) let-7a-complexed MCNP (MCNP/Let-7a); and (4) DOX-loaded and let-7a-complexed MCNP (MCNP-DOX/Let-7a). The four different treatment conditions were directly injected into the MDA-MB-231 tumors of mice every 3 days for 5 weeks. Each mouse received a particle dose of 5 mg/kg (DOX, 0.6 mg/kg; miRNA, 129.3 μg/kg) for each injection. (b) Tumor growth tracking in mice treated with the four different treatment conditions. Tumor volumes (cm^3) were assessed with calipers and are shown as means (n = 10 mice per group; *p < 0.0001). (c) Weight of the tumor tissues after combined let-7a and DOX treatment showed a significant decrease compared to the single treatment modality of either DOX or let-7a alone. The weight of MDA-MB-231 tumor tissues extracted from nude mice is shown as means ± standard deviation (n = 10, *p < 0.0001). (d) RT-qPCR analysis of tumor tissues showed the synergistic downregulation of the key targets involved in chemoresistance mechanisms (drug efflux and DNA repair) (n = 10; *p < 0.05, **p < 0.001).

in mice receiving injections. The MDA-MB-231 tumors were extracted and weighed after the whole course of treatment and showed that the combination therapy significantly reduced tumor weight when compared to nontreated and treated with single modality treatments (Figure 4c). These results demonstrate that let-7a can be used to enhance the anticancer effects of DOX in an in vivo xenograft model of breast cancer.

From qPCR analysis, we speculate that this unique combination (e.g., let-7a with DOX) acts primarily through the downregulation of drug efflux pumps, DNA repair mechanisms, and inhibition of tumor proliferation and prosurvival pathways. In particular, let-7a codelivery can simultaneously downregulate multiple genes, including members of the RAS family, HMGA2, ABCG2, and BRCA2, to induce caspase-3-mediated apoptosis (Figures 4d and S6), which is in agreement with previous reports.[14,15] As a result, MCNP-based codelivery of miRNA was able to sensitize triple-negative breast cancer cells to the treatment of DOX, which released from the pores of the mSi shell of our MCNPs.

Although therapeutically promising, in vivo toxicity and clearance of the core−shell magnetic mSi nanoparticles remain a concern.[59] Although magnetic nanoparticles and silica materials have been approved by the US Food and Drug Administration (FDA) for clinical use, it should not be assumed that magnetic-mSi core−shell structures have an equivalent safety profile without further study.[60,61] One area of concern is the size of the nanoparticles, which can limit clearance. This results in the accumulation of these particles, which over the long-term may cause damage to tissues and organs.[62] To overcome this issue, one strategy is to exploit biodegradable silica, which can be engineered to degrade fully under biological conditions.[63] Because nanoparticles possess highly versatile surfaces and interior chemistries, as the exact parameters that affect the clearance of nanoparticles from the body are further elucidated, it will become significantly easier to construct nanocarriers with favorable pharmacological properties, thus enhancing the clinical potential of nanoplatforms.

CONCLUSIONS

In this work, we have successfully demonstrated that the combination of let-7a and DOX chemotherapy can act as a potent therapy for cancer by overcoming chemoresistance. In particular, we have developed MCNPs consisting of a highly magnetic core and a biocompatible mSi shell, wherein DOX was loaded in the pores of the mSi shell, whereas let-7a was complexed on the surface through electrostatic interaction, resulting in the simultaneous delivery of these orthogonal modalities. We found that the treatment of triple-negative breast cancer cells (e.g., MDA-MB-231) with our combination therapy resulted in a synergistic decrease in cell viability, wherein 100 μg/mL of this combination therapy was able to decrease cell viability by over 90% in vitro and decreased tumor volume by 85% from in vivo model, which is significantly greater than either treatment modality alone.

Previous studies have developed similar platforms, where siRNAs targeting multidrug resistance genes (e.g., multidrug resistance-associated protein-1, MRP1) or prosurvival pathways (e.g., B cell lymphoma 2, BCL2) can help overcome chemoresistance.[24,45,64] For instance, Meng et al. demonstrated that the delivery of siRNA against P-glycoprotein protein, a drug efflux transporter, can enhance treatment of drug-resistant KB-V1 cells in an additive or synergistic fashion in vitro.[65] This platform was also found to function in vivo to synergistically inhibit tumor growth.[66] Although promising, it is a well-known fact that cancer cells typically utilize more than one mechanism to circumvent chemotherapy-induced cytotoxicity, and as such, miRNA therapeutics having multitargets are required to treat chemoresistant cancers more effectively.

In conclusion, we have demonstrated an advanced MCNP-based platform that can be used to simultaneously deliver miRNA and chemotherapeutic agents to malignant tumors in a target-specific manner. In particular, we provided a comprehensive report on the combined use of let-7a and DOX chemotherapy. We have also further demonstrated the additional multifunctionality offered by the use of MCNPs, where MRI provides a mean to monitor particle delivery. Furthermore, this platform can potentially be combined with magnetic hyperthermia-based therapy, which can act in concert with let-7a to further sensitize cells to chemotherapy.[22] Overall, this result provides proof-of-concept for the delivery of miRNA/drug combinations using combinatorial nanocarriers to overcome chemoresistance.

DOI: 10.1021/acsami.8b09086
ACS Appl. Mater. Interfaces XXXX, XXX, XXX−XXX

ASSOCIATED CONTENT

Supporting Information

The Supporting Information is available free of charge on the ACS Publications website at DOI: 10.1021/acsami.8b09086.

Characterization of MCNPs (TEM images of the lattice structure, FTIR spectra of CTAB-removed mSi, size and zeta potential during the progression of layer-by-layer assembly on MCNPs, confirmation of phosphonate functionalization on mSi, and cytotoxicity of MCNPs); stability of MCNPs; qPCR analysis of MDA-MB-231 cells and xenografts; synthetic scheme of iRGD conjugation; and primer sequences for qPCR (PDF)

AUTHOR INFORMATION

Corresponding Author

*E-mail: kblee@rutgers.edu.

ORCID

Thanapat Pongkulapa: 0000-0003-0678-1736
Hyeon-Yeol Cho: 0000-0003-1897-1166
Jeong-Woo Choi: 0000-0003-0100-0582

Author Contributions

¶P.T.Y. and T.P. contributed equally to this work.

Notes

The authors declare no competing financial interest.

ACKNOWLEDGMENTS

The work was partially supported by the NIH R01 (R01DC016612-01), the NIH R21 (R21AR071101-01), the NSF (CHE-1429062), the ACS (PRF# 55869-ND10), the N.J. Commission on Spinal Cord Research (CSCR16ERG019), and the National Research Foundation of Korea (NRF) [2013K1A4A3055268 and 2016R1A6A1A03012845, funded by the Ministry of Science, ICT and Future Planning (MSIP) and the Ministry of Education of Korea].

REFERENCES

(1) Marusyk, A.; Almendro, V.; Polyak, K. Intra-Tumour Heterogeneity: A Looking Glass for Cancer? *Nat. Rev. Cancer* **2012**, *12*, 323−334.

(2) Carey, L. A.; Dees, E. C.; Sawyer, L.; Gatti, L.; Moore, D. T.; Collichio, F.; Ollila, D. W.; Sartor, C. I.; Graham, M. L.; Perou, C. M. The Triple Negative Paradox: Primary Tumor Chemosensitivity of Breast Cancer Subtypes. *Clin. Cancer Res.* **2007**, *13*, 2329−2334.

(3) Voduc, K. D.; Cheang, M. C. U.; Tyldesley, S.; Gelmon, K.; Nielsen, T. O.; Kennecke, H. Breast Cancer Subtypes and The Risk of Local and Regional Relapse. *J. Clin. Oncol.* **2010**, *28*, 1684−1691.

(4) Hortobagyi, G. N. Treatment of Breast Cancer. *N. Engl. J. Med.* **1998**, *339*, 974−984.

(5) Gradishar, W. J. Taxanes for the Treatment of Metastatic Breast Cancer. *Breast Cancer: Basic Clin. Res.* **2012**, *6*, 159−171.

(6) Crown, J.; O'Leary, M.; Ooi, W. S. Docetaxel and Paclitaxel in the Treatment of Breast Cancer: A Review of Clinical Experience. *Oncologist* **2004**, *9*, 24−32.

(7) Holohan, C.; Van Schaeybroeck, S.; Longley, D. B.; Johnston, P. G. Cancer Drug Resistance: An Evolving Paradigm. *Nat. Rev. Cancer* **2013**, *13*, 714−726.

(8) Ha, M.; Kim, V. N. Regulation of MicroRNA Biogenesis. *Nat. Rev. Mol. Cell Biol.* **2014**, *15*, 509−524.

(9) Lin, S.; Gregory, R. I. MicroRNA Biogenesis Pathways in Cancer. *Nat. Rev. Cancer* **2015**, *15*, 321−333.

(10) He, L.; Hannon, G. J. Erratum: MicroRNAs: small RNAs with a big role in gene regulation. *Nat. Rev. Genet.* **2004**, *5*, 522−531.

(11) Sayed, D.; Abdellatif, M. MicroRNAs in Development and Disease. *Physiol. Rev.* **2011**, *91*, 827−887.

(12) Gangaraju, V. K.; Lin, H. MicroRNAs: Key Regulators of Stem Cells. *Nat. Rev. Mol. Cell Biol.* **2009**, *10*, 116−125.

(13) Davis-Dusenbery, B. N.; Hata, A. MicroRNA in Cancer: The Involvement of Aberrant MicroRNA Biogenesis Regulatory Pathways. *Genes Cancer* **2010**, *1*, 1100−1114.

(14) Barh, D.; Malhotra, R.; Ravi, B.; Sindhurani, P. MicroRNA let-7: An Emerging Next-Generation Cancer Therapeutic. *Curr. Oncol.* **2010**, *17*, 70−80.

(15) Boyerinas, B.; Park, S.-M.; Murmann, A. E.; Gwin, K.; Montag, A. G.; Zillhardt, M.; Hua, Y.-J.; Lengyel, E.; Peter, M. E. Let-7 Modulates Acquired Resistance of Ovarian Cancer to Taxanes via IMP-1-Mediated Stabilization of Multidrug Resistance 1. *Int. J. Cancer* **2012**, *130*, 1787−1797.

(16) Jang, J.-t.; Nah, H.; Lee, J.-H.; Moon, S. H.; Kim, M. G.; Cheon, J. Critical Enhancements of MRI Contrast and Hyperthermic Effects by Dopant-Controlled Magnetic Nanoparticles. *Angew. Chem., Int. Ed.* **2009**, *48*, 1234−1238.

(17) Kallumadil, M.; Tada, M.; Nakagawa, T.; Abe, M.; Southern, P.; Pankhurst, Q. A. Suitability of Commercial Colloids for Magnetic Hyperthermia. *J. Magn. Magn. Mater.* **2009**, *321*, 1509−1513.

(18) Kim, J.; Kim, H. S.; Lee, N.; Kim, T.; Kim, H.; Yu, T.; Song, I. C.; Moon, W. K.; Hyeon, T. Multifunctional Uniform Nanoparticles Composed of a Magnetite Nanocrystal Core and a Mesoporous Silica Shell for Magnetic Resonance and Fluorescence Imaging and for Drug Delivery. *Angew. Chem., Int. Ed.* **2008**, *47*, 8438−8441.

(19) Shah, B.; Yin, P. T.; Ghoshal, S.; Lee, K.-B. Multimodal Magnetic Core-Shell Nanoparticles for Effective Stem-Cell Differentiation and Imaging. *Angew. Chem., Int. Ed.* **2013**, *52*, 6190−6195.

(20) Shah, B. P.; Pasquale, N.; De, G.; Tan, T.; Ma, J.; Lee, K.-B. Core-Shell Nanoparticle-Based Peptide Therapeutics and Combined Hyperthermia for Enhanced Cancer Cell Apoptosis. *ACS Nano* **2014**, *8*, 9379−9387.

(21) Sun, S.; Zeng, H.; Robinson, D. B.; Raoux, S.; Rice, P. M.; Wang, S. X.; Li, G. Monodisperse MFe2O4(M = Fe, Co, Mn) Nanoparticles. *J. Am. Chem. Soc.* **2004**, *126*, 273−279.

(22) Yin, P. T.; Shah, B. P.; Lee, K. B. Combined Magnetic Nanoparticle-Based MicroRNA and Hyperthermia Therapy to Enhance Apoptosis in Brain Cancer Cells. *Small* **2014**, *10*, 4106−4112.

(23) Yin, P. T.; Shah, S.; Pasquale, N. J.; Garbuzenko, O. B.; Minko, T.; Lee, K.-B. Stem Cell-Based Gene Therapy Activated Using Magnetic Hyperthermia to Enhance the Treatment of Cancer. *Biomaterials* **2016**, *81*, 46−57.

(24) Chen, W.; Yuan, Y.; Cheng, D.; Chen, J.; Wang, L.; Shuai, X. Co-Delivery of Doxorubicin and siRNA with Reduction and pH Dually Sensitive Nanocarrier for Synergistic Cancer Therapy. *Small* **2014**, *10*, 2678−2687.

(25) Höbel, S.; Aigner, A. Polyethylenimines for siRNA and miRNA delivery in vivo. *Wiley Interdiscip. Rev.: Nanomed. Nanobiotechnol.* **2013**, *5*, 484−501.

(26) Chang, B.; Guo, J.; Liu, C.; Qian, J.; Yang, W. Surface Functionalization of Magnetic Mesoporous Silica Nanoparticles for Controlled Drug Release. *J. Mater. Chem.* **2010**, *20*, 9941−9947.

(27) Lai, J.; Shah, B. P.; Zhang, Y.; Yang, L.; Lee, K.-B. Real-Time Monitoring of ATP-Responsive Drug Release Using Mesoporous-Silica-Coated Multicolor Upconversion Nanoparticles. *ACS Nano* **2015**, *9*, 5234−5245.

(28) Elbakry, A.; Zaky, A.; Liebl, R.; Rachel, R.; Goepferich, A.; Breunig, M. Layer-by-Layer Assembled Gold Nanoparticles for siRNA Delivery. *Nano Lett.* **2009**, *9*, 2059−2064.

(29) Kim, W. J.; Yockman, J. W.; Lee, M.; Jeong, J. H.; Kim, Y.-H.; Kim, S. W. Soluble Flt-1 Gene Delivery using PEI-g-PEG-RGD Conjugate for Anti-Angiogenesis. *J. Controlled Release* **2005**, *106*, 224−234.

(30) Zhan, C.; Qian, J.; Feng, L.; Zhong, G.; Zhu, J.; Lu, W. Cyclic RGD-poly(ethylene glycol)-polyethyleneimine is more suitable for

DOI: 10.1021/acsami.8b09086
ACS Appl. Mater. Interfaces XXXX, XXX, XXX−XXX

glioblastoma targeting gene transferin vivo. *J. Drug Targeting* **2011**, *19*, 573−581.
(31) Spandidos, A.; Wang, X.; Wang, H.; Seed, B. PrimerBank: A Resource of Human and Mouse PCR Primer Pairs for Gene Expression Detection and Quantification. *Nucleic Acids Res.* **2010**, *38*, D792−D799.
(32) Spandidos, A.; Wang, X.; Wang, H.; Dragnev, S.; Thurber, T.; Seed, B. A Comprehensive Collection of Experimentally Validated Primers for Polymerase Chain Reaction Quantitation of Murine Transcript Abundance. *BMC Genomics* **2008**, *9*, 633.
(33) Wang, X.; Seed, B. A PCR Primer Bank for Quantitative Gene Expression Analysis. *Nucleic Acids Res.* **2003**, *31*, e154.
(34) Cho, H.-Y.; Hossain, M. K.; Lee, J.-H.; Han, J.; Lee, H. J.; Kim, K.-J.; Kim, J.-H.; Lee, K.-B.; Choi, J.-W. Selective Isolation and Noninvasive Analysis of Circulating Cancer Stem Cells Through Raman Imaging. *Biosens. Bioelectron.* **2018**, *102*, 372−382.
(35) Cho, H.-Y.; Lee, T.; Yoon, J.; Han, Z.; Rabie, H.; Lee, K.-B.; Su, W. W.; Choi, J.-W. Magnetic Oleosome as a Functional Lipophilic Drug Carrier for Cancer Therapy. *ACS Appl. Mater. Interfaces* **2018**, *10*, 9301−9309.
(36) Ye, F.; Laurent, S.; Fornara, A.; Astolfi, L.; Qin, J.; Roch, A.; Martini, A.; Toprak, M. S.; Muller, R. N.; Muhammed, M. Uniform mesoporous silica coated iron oxide nanoparticles as a highly efficient, nontoxic MRI T2 contrast agent with tunable proton relaxivities. *Contrast Media Mol. Imaging* **2012**, *7*, 460−468.
(37) Horcajada, P.; Rámila, A.; Férey, G.; Vallet-Regí, M. Influence of Superficial Organic Modification of MCM-41 Matrices on Drug Delivery Rate. *Solid State Sci.* **2006**, *8*, 1243−1249.
(38) Che, E.; Wan, L.; Zhang, Y.; Zhao, Q.; Han, X.; Li, J.; Liu, J.; Wang, S. Development of Phosphonate-Terminated Magnetic Mesoporous Silica Nanoparticles for pH-Controlled Release of Doxorubicin and Improved Tumor Accumulation. *Asian J. Pharm. Sci.* **2014**, *9*, 317−323.
(39) Wightman, L.; Kircheis, R.; Rössler, V.; Carotta, S.; Ruzicka, R.; Kursa, M.; Wagner, E. Different behavior of branched and linear polyethylenimine for gene deliveryin vitro andin vivo. *J. Gene Med.* **2001**, *3*, 362−372.
(40) Kunath, K.; von Harpe, A.; Fischer, D.; Petersen, H.; Bickel, U.; Voigt, K.; Kissel, T. Low-Molecular-Weight Polyethylenimine as a Non-Viral Vector for DNA Delivery: Comparison of Physicochemical Properties, Transfection Efficiency and In Vivo Distribution with High-Molecular-Weight Polyethylenimine. *J. Controlled Release* **2003**, *89*, 113−125.
(41) Delyagina, E.; Schade, A.; Scharfenberg, D.; Skorska, A.; Lux, C.; Li, W.; Steinhoff, G. Improved Transfection in Human Mesenchymal Stem Cells: Effective Intracellular Release of pDNA by Magnetic Polyplexes. *Nanomedicine* **2014**, *9*, 999−1017.
(42) Sun, S.; Wang, Y.; Zhou, R.; Deng, Z.; Han, Y.; Han, X.; Tao, W.; Yang, Z.; Shi, C.; Hong, D.; Li, J.; Shi, D.; Zhang, Z. Targeting and Regulating of an Oncogene via Nanovector Delivery of MicroRNA using Patient-Derived Xenografts. *Theranostics* **2017**, *7*, 677−693.
(43) Wang, Z.; Chang, Z.; Lu, M.; Shao, D.; Yue, J.; Yang, D.; Zheng, X.; Li, M.; He, K.; Zhang, M.; Chen, L.; Dong, W.-f. Shape-Controlled Magnetic Mesoporous Silica Nanoparticles for Magnetically-Mediated Suicide Gene Therapy of Hepatocellular Carcinoma. *Biomaterials* **2018**, *154*, 147−157.
(44) Kennedy, R. D.; Quinn, J. E.; Mullan, P. B.; Johnston, P. G.; Harkin, D. P. The Role of BRCA1 in the Cellular Response to Chemotherapy. *JNCI, J. Natl. Cancer Inst.* **2004**, *96*, 1659−1668.
(45) Dönmez, Y.; Gündüz, U. Reversal of Multidrug Resistance By Small Interfering RNA (siRNA) in Doxorubicin-Resistant MCF-7 Breast Cancer Cells. *Biomed. Pharmacother.* **2011**, *65*, 85−89.
(46) Garrido, C.; Solary, E. A role of HSPs in apoptosis through "protein triage"? *Cell Death Differ.* **2003**, *10*, 619−620.
(47) Takayama, S.; Reed, J. C.; Homma, S. Heat-Shock Proteins as Regulators of Apoptosis. *Oncogene* **2003**, *22*, 9041−9047.
(48) Johnson, S. M.; Grosshans, H.; Shingara, J.; Byrom, M.; Jarvis, R.; Cheng, A.; Labourier, E.; Reinert, K. L.; Brown, D.; Slack, F. J. RAS is Regulated By The Let-7 MicroRNA Family. *Cell* **2005**, *120*, 635−647.
(49) Zhu, H.; Shyh-Chang, N.; Segrè, A. V.; Shinoda, G.; Shah, S. P.; Einhorn, W. S.; Takeuchi, A.; Engreitz, J. M.; Hagan, J. P.; Kharas, M. G.; Urbach, A.; Thornton, J. E.; Triboulet, R.; Gregory, R. I.; Altshuler, D.; Daley, G. Q. The Lin28/Let-7 Axis Regulates Glucose Metabolism. *Cell* **2011**, *147*, 81−94.
(50) Johnson, C. D.; Esquela-Kerscher, A.; Stefani, G.; Byrom, M.; Kelnar, K.; Ovcharenko, D.; Wilson, M.; Wang, X.; Shelton, J.; Shingara, J.; Chin, L.; Brown, D.; Slack, F. J. The Let-7 MicroRNA Represses Cell Proliferation Pathways in Human Cells. *Cancer Res.* **2007**, *67*, 7713−7722.
(51) Yu, F.; Yao, H.; Zhu, P.; Zhang, X.; Pan, Q.; Gong, C.; Huang, Y.; Hu, X.; Su, F.; Lieberman, J.; Song, E. Let-7 Regulates Self Renewal and Tumorigenicity of Breast Cancer Cells. *Cell* **2007**, *131*, 1109−1123.
(52) Boyerinas, B.; Park, S.-M.; Hau, A.; Murmann, A. E.; Peter, M. E. The Role of Let-7 in Cell Differentiation and Cancer. *Endocr.-Relat. Cancer* **2010**, *17*, 19−36.
(53) Lucie, S.; Elisabeth, G.; Stéphanie, F.; Guy, S.; Amandine, H.; Corinne, A.-R.; Didier, B.; Catherine, S.; Alexeï, G.; Pascal, D.; Jean-Luc, C. Clustering and Internalization of Integrin $\alpha v\beta 3$ with a Tetrameric RGD-Synthetic Peptide. *Mol. Ther.* **2009**, *17*, 837−843.
(54) Knop, K.; Hoogenboom, R.; Fischer, D.; Schubert, U. S. Poly(Ethylene Glycol) in Drug Delivery: Pros and Cons as well as Potential Alternatives. *Angew. Chem., Int. Ed.* **2010**, *49*, 6288−6308.
(55) Sugahara, K. N.; Teesalu, T.; Karmali, P. P.; Kotamraju, V. R.; Agemy, L.; Girard, O. M.; Hanahan, D.; Mattrey, R. F.; Ruoslahti, E. Tissue-Penetrating Delivery of Compounds and Nanoparticles into Tumors. *Cancer Cell* **2009**, *16*, 510−520.
(56) Chattopadhyay, N.; Chatterjee, A. Studies on the Expression of Alpha(V)Beta3 Integrin Receptors in Non-Malignant and Malignant Human Cervical Tumor Tissues. *J. Exp. Clin. Cancer Res.* **2001**, *20*, 269−275.
(57) Murugan, C.; Rayappan, K.; Thangam, R.; Bhanumathi, R.; Shanthi, K.; Vivek, R.; Thirumurugan, R.; Bhattacharyya, A.; Sivasubramanian, S.; Gunasekaran, P.; Kannan, S. Combinatorial Nanocarrier Based Drug Delivery Approach for Amalgamation of Anti-Tumor Agents in Breast Cancer Cells: An Improved Nanomedicine Strategies. *Sci. Rep.* **2016**, *6*, 34053.
(58) Shao, D.; Li, J.; Zheng, X.; Pan, Y.; Wang, Z.; Zhang, M.; Chen, Q.-X.; Dong, W.-F.; Chen, L. Janus "nano-bullets" for magnetic targeting liver cancer chemotherapy. *Biomaterials* **2016**, *100*, 118−133.
(59) Longmire, M.; Choyke, P. L.; Kobayashi, H. Clearance Properties of Nano-Sized Particles and Molecules as Imaging Agents: Considerations and Caveats. *Nanomedicine* **2008**, *3*, 703−717.
(60) Chan, W.-T.; Liu, C.-C.; Chiang Chiau, J.-S.; Tsai, S.-T.; Liang, C.-K.; Cheng, M.-L.; Lee, H.-C.; Yeung, C.-Y.; Hou, S.-Y. In Vivo Toxicologic Study of Larger Silica Nanoparticles in Mice. *Int. J. Nanomed.* **2017**, *12*, 3421−3432.
(61) Mahmoudi, M.; Hofmann, H.; Rothen-Rutishauser, B.; Petri-Fink, A. Assessing the In Vitro and In Vivo Toxicity of Superparamagnetic Iron Oxide Nanoparticles. *Chem. Rev.* **2012**, *112*, 2323−2338.
(62) Berce, C.; Lucan, C.; Petrushev, B.; Boca, S.; Miclean, M.; Sarpataki, O.; Astilean, S.; Buzoianu, A.; Tomuleasa, C.; Bojan, A. In Vivo Assessment of Bone Marrow Toxicity by Gold Nanoparticle-Based Bioconjugates in Crl:CD1(ICR) Mice. *Int. J. Nanomed.* **2016**, *11*, 4261−4273.
(63) Croissant, J. G.; Fatieiev, Y.; Khashab, N. M. Degradability and Clearance of Silicon, Organosilica, Silsesquioxane, Silica Mixed Oxide, and Mesoporous Silica Nanoparticles. *Adv. Mater.* **2017**, *29*, 1604634.
(64) Chen, A. M.; Zhang, M.; Wei, D.; Stueber, D.; Taratula, O.; Minko, T.; He, H. Co-Delivery of Doxorubicin and Bcl-2 siRNA by Mesoporous Silica Nanoparticles Enhances the Efficacy of Chemotherapy in Multidrug-Resistant Cancer Cells. *Small* **2009**, *5*, 2673−2677.

DOI: 10.1021/acsami.8b09086
ACS Appl. Mater. Interfaces XXXX, XXX, XXX−XXX

(65) Meng, H.; Liong, M.; Xia, T.; Li, Z.; Ji, Z.; Zink, J. I.; Nel, A. E. Engineered Design of Mesoporous Silica Nanoparticles to Deliver Doxorubicin and P-Glycoprotein siRNA to Overcome Drug Resistance in a Cancer Cell Line. *ACS Nano* **2010**, *4*, 4539−4550.
(66) Meng, H.; Mai, W. X.; Zhang, H.; Xue, M.; Xia, T.; Lin, S.; Wang, X.; Zhao, Y.; Ji, Z.; Zink, J. I.; Nel, A. E. Codelivery of an Optimal Drug/siRNA Combination Using Mesoporous Silica Nanoparticles to Overcome Drug Resistance in Breast Cancer In Vitro and In Vivo. *ACS Nano* **2013**, *7*, 994−1005.

DOI: 10.1021/acsami.8b09086
ACS Appl. Mater. Interfaces XXXX, XXX, XXX−XXX